DALTON

Molecular manganese sulfide clusters formed by laser ablation†

Ian G. Dance,* Keith J. Fisher* and Gary D. Willett

School of Chemistry, University of New South Wales, Sydney 2052, Australia

Laser ablation of solid MnS yields in the gas phase polysulfane cations $[MnS_n]^+$ ($4 \leqslant n \leqslant 11$), and anionic clusters $[Mn_xS_x]^-$ and $[Mn_xS_{x+1}]^-$ ($2 \leqslant x \leqslant 22$), together with clusters $[Mn_xS_xO]^-$ ($4 \leqslant x \leqslant 22$) formed from adventitious water. These ions were detected and investigated further by Fourier-transform ion cyclotron resonance mass spectrometry. There are no major discontinuities in abundance or especially stable structures in the series $[Mn_xS_x]^-$ and $[Mn_xS_{x+1}]^-$. There are some differences in the distributions of ions formed by the pink and green forms of solid MnS, with the pink form generating more sulfur vapour and polysulfane cations, and the green form more suitable for the formation of cluster anions. The cations $[MnS_n]^+$ lose S_2 on collisional activation. The cluster anions $[Mn_xS_y]^-$ are generally unreactive and not oxidised by N_2O, but on reaction with H_2S (g) they undergo protonation or add one or two S atoms to form also the new products $[Mn_xS_{x+2}]^-$ ($4 \leqslant x \leqslant 8$). The compositions $[Mn_xS_x]^-$ and $[Mn_xS_{x+1}]^-$ represent a well defined region of stability for anions, and for the neutral clusters from which they are believed to be formed by electron attachment.

As part of our research on metal chalcogenide chemistry and clusters,[1–12] we have a program of investigation of the pristine metal chalcogenide clusters $[M_xE_y]$ (E = S, Se or Te) free of heteroligands.[1–4,6,11] This is achieved by formation and investigation of these clusters in the gas phase, where they are also devoid of the influences of solvent or crystal environments.[10] The results of this work provide fundamental reference data, as well as revealing possibilities for the preparation of new metal chalcogenide clusters and materials in condensed phases.

We use the technique of laser ablation (LA) coupled with Fourier-transform ion cyclotron resonance (FTICR) mass spectrometry, which allows all of the main operations of synthesis and characterisation. Synthesis is achieved by association of atoms and ions in a cooling plasma generated by the laser ablation of a solid precursor. The ionised products are collected in an ion trap, monitored mass spectrometrically as a function of time, and purified by removal of unwanted ions from the trap. Selected products thus isolated in the ion trap are further characterised by their reactions with other molecules in the gas phase, and by their dissociative processes: the temporal evolution of the distribution of ions can be monitored throughout. There is a correspondence between these experiments and the conventional investigatory sequence of synthesis ⟶ separation/purification ⟶ reactivity and reactions.[9–11]

The very large number of metal sulfide cluster anions $[M_xS_y]^-$ which can be generated and investigated this way is striking: by laser ablation of CoS, 83 new anionic molecules containing only Co and S ranging in size up to $[Co_{38}S_{24}]^-$ were detected.[4] We have reported also the $[M_xE_y]^-$ cluster ions formed by iron,[4] nickel,[1] copper[2] and silver,[3] and in this paper we describe the formation, distribution, and reactions of $[Mn_xS_y]^-$ molecular clusters.

In previous investigations the distribution of ions $[M_xE_y]^-$ and their relative abundances were largely independent of the composition of the solid precursor used in the laser ablation, and in some cases mixtures of the relevant elements yield the same distribution of ions $[M_xE_y]^-$. Thus NiS (s) and Ni_3S_2 (s) yielded essentially the same spectrum of $[Ni_xS_y]^-$; Cu_2S (s) and KCu_4S_3 (s) yielded similar collections of $[Cu_xS_y]^-$, and Cu_2Se (s) and a mixture of Cu (s) plus Se (s) gave very similar distributions $[Cu_xSe_y]^-$. Therefore we expected that laser ablation of two of the forms of manganese sulfide, green MnS and pink (metastable) MnS, would yield very similar gas phase species, but there are differences which we describe and rationalise in this paper. Some thermochemical data are available for MnS, MnS_2 and MnS_3.[13]

Experimental

Pink MnS was prepared by the reaction of H_2S with an oxygen-free aqueous buffer solution (NH_4Cl–NH_3) of a manganese(II) salt.[14] The precipitated sulfide was washed with an aqueous ammonium sulfide solution, then water and dried under vacuum. Green MnS was prepared by the reaction of H_2S with an oxygen-free ammoniacal solution of a manganese(II) salt in the presence of oxalate,[14] and washed and dried in the same way as the pink solid. Infrared spectra indicated the presence of water in both samples even after prolonged drying under vacuum (0.2 mmHg ≈ 26.6 Pa) at 50 °C.

LA-FTICR

Mass spectra were obtained using a Spectrospin CMS-47 FTICR mass spectrometer, equipped with a 4.7 T superconducting magnet.[1,4,9] The manganese sulfide powder was pressed into a satellite probe tip and introduced into the ICR cell using a direct insertion probe. A cylindrical ICR cell (radius 30 × 60 mm) with six titanium single section plates was used in an ultra high vacuum chamber maintained at a base pressure of 10^{-9} mbar by a turbomolecular pump. Cations or anions were trapped in the cell by potentials of +4 or −4 V on the end plates.

Laser ablation was performed using a Nd-YAG laser (1064 nm, Spectra Physics DCR-11) focused to an area of diameter 0.4 mm on the probe at the end of the cell, flush and in contact with the ICR trapping plate. The laser was used in the Q-switched mode producing a pulse for 8 ns, with laser power densities at the sample of 500–3000 MW cm^{-2}. The pulse energy at the sample was modified using neutral density filters.

Three types of LA-FTICR experiment were employed:[9] (*a*) measurement of broad band mass spectra and high resolution mass spectra; (*b*) dissociation of selected ions by controllably energised collisions with inert gas; (*c*) monitoring reactions of selected ions with H_2S gas. In each experiment there was an initial RF pulse of 5 ms to purge the cell of ions, followed after a delay of 0.01 s by the laser pulse. A delay period ranging from 100 ms to 1 s followed the laser pulse to allow cooling of the

† *Non-SI unit employed:* 1 bar = 10^5 Pa.

plasma and thermalisation of the products: the variation of this delay was used also to investigate relative stabilities of the product ions. Observation of the broad band spectrum of the products at this stage used an excitation RF pulse and after a delay of 0.5–2 ms the signal induced in the receiver plates was acquired and processed. In measurements of the collisional dissociation (type *b*) or of the ion–molecule reactions (type *c*), an ejection pulse of 35–50 μs was used 100 ms after the laser pulse, in order to remove all but the target ion to be studied. Collisional dissociation (type *b*) was induced by acceleration of the ions in the presence of inert gas (Ar) at 10^{-7} mbar: the acceleration pulse was increased in duration until dissociation products were detected (after a constant delay of 10 ms). In the ion–molecule reactions (type *c*), laser ablation was performed in the presence of H_2S at a background pressure of 10^{-7} mbar. After the ejection of all ions other than the $[Mn_xS_y]^-$ to be investigated, a variable period was allowed for reaction, followed by the detection sequence as described above. High mass ions could often not be selected cleanly using varying ejection pulses and higher mass ions were detected to be present. These higher mass ions did not interfere in the measurement of collisional dissociations, as the acceleration pulse prior to detection was observed to affect only the selected ion.

The presence and amount of oxygen in some ions was determined by accurate measurement of the isotopic pattern, to remove ambiguities due to the related masses of S and O. The intensity of the (Q + 2) ion relative to that of the Q ion (Q is the molecular ion) is decisive: as illustration, for $Mn_{12}S_{12}O$ the measured relative intensity for the Q + 2 ion is 55.1%, calculated 53.9%, compared with 49.8% calculated for $Mn_{12}S_{11}O_3$.

Results

The products of laser ablation

Freshly prepared pink MnS (s) possessed a background vapour of sulfur molecules, as revealed by the ions $[S_n]^+$ (n = 5, 6 or 8) generated by electron impact (EI) ionisation without any laser ablation of the solid. Laser ablation of the pink MnS gave high intensities of $[S_n]^+$ ions, and Mn^+ and $[MnS_n]^+$ ions (n = 4–11) were observed from several samples. Increased delay between laser ablation of the solid and observation of the ions increased the abundances of $[MnS_n]^+$and decreased Mn^+: $[MnS_4]^+$ was the most intense positive ion in the spectrum when the ions were observed 1 s after ablation. These results are consistent with our separate studies of EI spectra of S_8, and of the $Mn^+ + S_8$ (g) reaction,[7,9] and are explained by the presence of S_8 and Mn on the surface of pink MnS. The positive ion spectra of laser ablated green MnS were dominated by Mn^+ and a few $[S_n]^+$ ions, without the $[MnS_n]^+$ even after long periods between ablation and observation.

The negative ion spectra of pink MnS (s) were dominated by the $[S_n]^-$ ions (n = 3–6), and contained $[Mn_xS_y]^-$ ions of lower intensity. The most abundant cluster ions were $[Mn_4S_4O]^-$ and $[Mn_4S_5]^-$. The oxygen appearing in this and related clusters is adventitious, from water retained even after strong drying of the samples.

Laser ablation of freshly prepared green MnS (s) generated a richer collection of negative clusters, with compositions $[Mn_xS_x]^-$ and $[Mn_xS_{x+1}]^-$, and some $[Mn_xS_xO]^-$ ions ($x \leqslant 22$). Fig. 1 shows a typical spectrum, the ions observed are listed in Table 1, and the distribution of ions is presented clearly in the ion map of Fig. 2. Aged samples of green MnS stored under nitrogen gave spectra with a greater abundance of sulfur ions $[S_n]^-$ and a much lower intensity of the high mass $[Mn_xS_y]^-$ ions.

For both pink and green MnS (s) the spectra after laser ablation are largely independent of the ablation history of the samples. The first laser pulse liberates larger amounts of S_n,

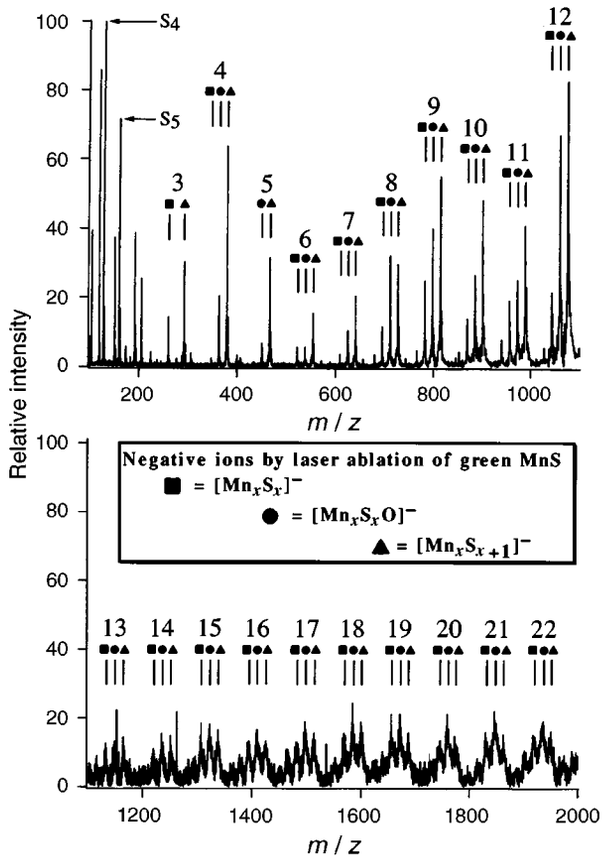

Fig. 1 Spectrum of negative ions formed by laser ablation of freshly prepared green MnS

Table 1 The $[Mn_xS_y]^-$ ions formed on laser ablation of freshly prepared green MnS

Ion	*m/z*	Intensity	Ion	*m/z*	Intensity
MnS_2	119	86	$Mn_{13}S_{13}O$	1146	13
MnS_3	151	37	$Mn_{13}S_{14}$	1162	14
Mn_2S_3	206	25	$Mn_{14}S_{14}$	1217	11
Mn_3S_3	261	14	$Mn_{14}S_{14}O$	1233	15
Mn_3S_4	293	30	$Mn_{14}S_{15}$	1249	15
Mn_4S_4	348	2	$Mn_{15}S_{14}O$	1288	9
Mn_4S_4O	364	20	$Mn_{15}S_{15}$	1304	18
Mn_4S_5	380	63	$Mn_{15}S_{15}O$	1320	18
Mn_5S_5O	451	7	$Mn_{15}S_{16}$	1336	16
Mn_5S_6	467	32	$Mn_{16}S_{16}$	1391	13
Mn_6S_6	521	10	$Mn_{16}S_{16}O$	1407	17
Mn_6S_6O	537	8	$Mn_{16}S_{17}$	1423	13
Mn_6S_7	553	11	$Mn_{17}S_{16}O$	1461	11
Mn_7S_7O	624	10	$Mn_{17}S_{17}$	1477	13
Mn_7S_8	640	20	$Mn_{17}S_{17}O$	1493	19
Mn_8S_8	695	12	$Mn_{17}S_{18}$	1509	16
Mn_8S_8O	711	32	$Mn_{18}S_{17}O$	1548	9
Mn_8S_9	727	30	$Mn_{18}S_{18}$	1564	15
Mn_9S_9	782	25	$Mn_{18}S_{18}O$	1580	24
Mn_9S_9O	798	40	$Mn_{18}S_{19}$	1596	19
Mn_9S_{10}	814	55	$Mn_{19}S_{19}$	1651	21
$Mn_{10}S_{10}$	869	14	$Mn_{19}S_{19}O$	1667	21
$Mn_{10}S_{10}O$	885	26	$Mn_{19}S_{20}$	1683	16
$Mn_{10}S_{11}$	901	48	$Mn_{20}S_{20}$	1738	14
$Mn_{11}S_{10}O$	940	8	$Mn_{20}S_{20}O$	1754	21
$Mn_{11}S_{11}$	956	19	$Mn_{20}S_{21}$	1770	15
$Mn_{11}S_{11}O$	972	25	$Mn_{21}S_{21}$	1825	16
$Mn_{11}S_{12}$	988	41	$Mn_{21}S_{21}O$	1841	22
$Mn_{12}S_{12}$	1043	22	$Mn_{21}S_{22}$	1857	15
$Mn_{12}S_{12}O$	1059	67	$Mn_{22}S_{21}O$	1896	11
$Mn_{12}S_{13}$	1075	83	$Mn_{22}S_{22}$	1912	15
$Mn_{13}S_{12}O$	1114	9	$Mn_{22}S_{22}O$	1928	19
$Mn_{13}S_{13}O$	1130	13	$Mn_{22}S_{23}$	1944	16

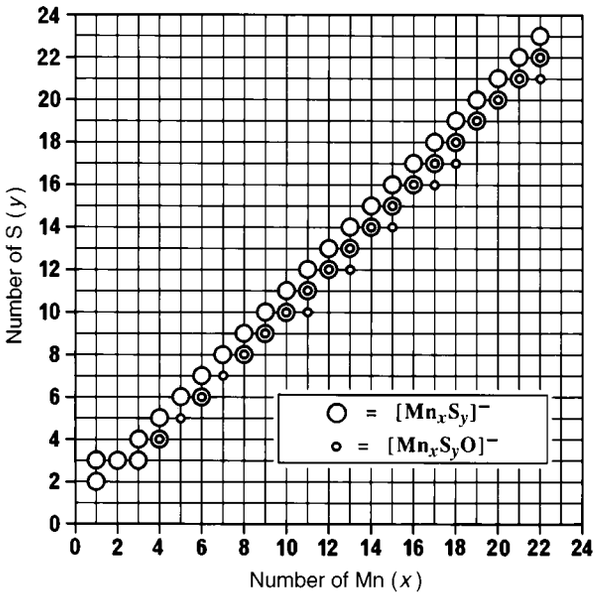

Fig. 2 Map of the compositions of the ions $[Mn_xS_y]^-$ and $[Mn_xS_yO]^-$ formed by laser ablation of freshly prepared green MnS

observable as positive or negative ions, but thereafter the spectra did not change appreciably with repeated laser pulses.

Collisionally-induced dissociation

The collisionally-induced dissociations of the $[MnS_n]^+$ ions generated from pink MnS are summarised in Table 2. Loss of S_2 is a common process. The products of collisionally-induced dissociation of the $[Mn_xS_y]^-$ ions from green MnS are summarised in Table 3. Several ions, $[Mn_3S_3]^-$, $[Mn_5S_6]^-$, $[Mn_7S_8]^-$, $[Mn_8S_9]^-$ and $[Mn_9S_{10}]^-$, did not give any dissociative product ions but were observed to decrease in intensity with increasing energy of the colliding argon atoms. This is interpreted as collisionally-induced loss of an electron to form the neutral species of the same formula. It is possible that there may be dissociation accompanying electron loss but our experiment cannot detect neutral products of such processes.

Reactions of $[Mn_xS_y]^-$ ions with H_2S

The manganese sulfide ions $[Mn_xS_y]^-$ were observed to be unreactive with the oxidant N_2O. They did react with H_2S at 10^{-7} mbar, resulting in the addition of one sulfur atom, and in some cases two sulfur atoms. The main reaction products are summarised below:

$$[Mn_2S_3]^- \longrightarrow [Mn_2S_4]^-$$
$$[Mn_3S_3]^- \longrightarrow [Mn_3S_4]^- \longrightarrow [Mn_3S_5]^-$$
$$[Mn_4S_4]^- \longrightarrow [Mn_4S_5]^- \longrightarrow [Mn_4S_6]^-$$
$$[Mn_5S_6]^- \longrightarrow [Mn_5S_7]^-$$
$$[Mn_6S_6]^- \longrightarrow [Mn_6S_7]^- \longrightarrow [Mn_6S_8]^-$$
$$[Mn_7S_8]^- \longrightarrow [Mn_7S_9]^-$$
$$[Mn_8S_9]^- \longrightarrow [Mn_8S_{10}]^-$$
$$[Mn_9S_9]^- \longrightarrow [Mn_9S_{10}]^-$$

Experimental difficulties precluded measurement of reactions for larger ions.

The reactions $[Mn_xS_x]^- + H_2S \longrightarrow [Mn_xS_{x+1}]^-$ generate clusters which are observed directly in the laser ablation of MnS, but the products $[Mn_xS_{x+2}]^-$ (x = 4–8) formed by reaction with H_2S are new. Small amounts of the proton exchange product HS^- were almost always present, implying the occurrence of reactions $[Mn_xS_y]^- + H_2S \longrightarrow [Mn_xS_yH] + HS^-$.

Table 2 Products of collisionally induced dissociation of $[MnS_n]^+$

Ion	Dissociation products
$[MnS_3]^+$	$[MnS_2]^+ + Mn^+$
$[MnS_4]^+$	$[MnS_2]^+ + [MnS]^+ + Mn^+$
$[MnS_5]^+$	$[MnS_3]^+ + [MnS_2]^+ + [MnS]^+ + Mn^+$
$[MnS_6]^+$	$[MnS_4]^+ + [MnS_2]^+ + Mn^+$
$[MnS_8]^+$	$[MnS_6]^+ + [MnS_4]^+ + [MnS_2]^+$

Table 3 Results of the collisionally induced dissociation of $[Mn_xS_y]^-$ ions

Ion	Daughter product ions	Neutral fragment lost
$Mn_2S_3^-$	MnS_3^-	Mn
$Mn_3S_3^-$	No observed ions	Mn_3S_3 (charge loss)
$Mn_3S_4^-$	MnS_2^-, $Mn_3S_3^-$	Mn_2S_2, S
$Mn_4S_5^-$	MnS_2^-	Mn_3S_3
$Mn_5S_6^-$	No observed ions	Mn_5S_6 (charge loss)
$Mn_6S_7^-$	$Mn_6S_6^-$	S
$Mn_7S_8^-$	No observed ions	Mn_7S_8 (charge loss)
$Mn_8S_9^-$	No observed ions	Mn_8S_9 (charge loss)
$Mn_9S_{10}^-$	No observed ions	Mn_9S_{10} (charge loss)
$Mn_{10}S_{11}^-$	$Mn_9S_{10}^-$	MnS
$Mn_{11}S_{12}^-$	$Mn_{10}S_{11}^-$	MnS
$Mn_{12}S_{13}^-$	$Mn_{11}S_{12}^-$	MnS
$Mn_4S_4O^-$	MnS_4^-, S^-, S_2^-, S_3^-	Mn_3O, Mn_4S_3O, Mn_4S_2O, Mn_4SO

Discussion

The green (α) form of MnS has a cubic rock salt structure with MnS_6 local co-ordination, and is more stable than the two pink modifications which have tetrahedral MnS_4 co-ordination in the zinc blende (cubic) and wurtzite (hexagonal) lattices. Conversion of pink to green occurs above the relatively low temperature of 200 °C.[15–18] When precipitated from aqueous solution the pink forms are often hydrated.

Laser ablation and the generation of gaseous clusters

We begin with discussion of the processes occurring during the laser ablation of these solids, as revealed by the FTICR spectra. The laser ablation process generates very high temperatures at the surface of the solid. However, even without laser ablation the loss of sulfur vapour from the surface of pink MnS is evident from the low energy electron impact mass spectrometry. After ablation, the excess sulfur associated with pink MnS is evident in the positive ions $[S_n]^+$, the negative ions $[S_n]^-$ (n mainly 3 or 6), and the ions $[MnS_4]^+$, $[MnS_8]^+$ and $[MnS_{11}]^+$. These $[MnS_n]^+$ ions are formed in the same sequence in the reactions Mn^+ (g) + S_8 (g) investigated independently,[7,9] and so observation of them on ablation of pink MnS is indication that Mn^+ and S_8 are generated at the surface.

Green MnS yields fewer $[S_n]^+$ ions and no $[MnS_n]^+$ ions, but does form a richer collection of negative cluster ions than does pink MnS. There are three series of related ions with the general formulas $[Mn_xS_x]^-$, $[Mn_xS_{x+1}]^-$ and $[Mn_xS_xO]^-$, up to x = 22 as emphasised in Fig. 2. The most intense ions are $[MnS_2]^-$, $[Mn_4S_5]^-$ and $[Mn_{12}S_{13}]^-$, and there are notable absences of $[Mn_5S_5]^-$ and $[Mn_7S_7]^-$. In general, ions in the series $[Mn_xS_{x+1}]^-$ are more abundant than those in the $[Mn_xS_x]^-$ series, for similar x. Very few $[Mn_xS_y]^-$ ions outside of the series $[Mn_xS_x]^-$ and $[Mn_xS_{x+1}]^-$ are evident. The oxygen in the ions of the series $[Mn_xS_xO]^-$ is adventitious, but oxygen contamination of samples of MnS (s) is well known.[19] Parent[20] observed similar oxygen presence in the positive ions formed by laser ablation of aluminium sulfide.

In summary, the differences in the ions formed for the two solid forms of MnS (which are largely independent of the ablation histories of the samples) are:

pink MnS ⟶ positive ions $[S_n]^+$, Mn^+, $[MnS_y]^+$

green MnS ⟶ few positive ions $[S_n]^+$

pink MnS ⟶ negative ions $[S_n]^-$, few $[Mn_xS_y]^-$

green MnS ⟶ many negative ions $[Mn_xS_y]^-$

These differences are due to the different stabilities of the two solids. Pink MnS decomposes to sulfur vapour at its surface, a process accentuated by laser ablation, and the sulfur vapour traps electrons to form ions $[S_n]^-$. The electron affinity of S_3 is 2.09 eV ($\approx 3.34 \times 10^{-19}$ J).[21,22] Consequently the yield of $[Mn_xS_y]^-$ ions from pink MnS is reduced relative to the abundance and range of $[Mn_xS_y]^-$ ions generated by laser ablation of the more stable green form. The surface temperature of the solid during laser impact, estimated to be several thousand degrees, is very much higher than the transition temperature (200 °C) for conversion of pink MnS to the green form, but the rate of conversion is too slow to have any influence during the millisecond periods during which the gaseous species are generated in our experiments.

The dependence of the distribution of products on the identity of the MnS solid being ablated is contrary to previous results for other metal chalcogenides. In the laser ablation of KCu_3S_4, CuS or Cu_2S, each gave similar distributions of $[Cu_xS_y]^-$ with a few exceptions: mixtures in different proportions of elemental copper with elemental selenium or tellurium have distributions of $[Cu_xE_y]^-$ which were the same as those of CuSe or CuTe.[2] However, previous precursors for the generation of cluster anions $[M_xS_y]^-$ did not introduce sulfur vapour, as occurs with the use of pink MnS. We believe that in laser ablation mass spectrometry of metal chalcogenides the resulting ions do not reflect the composition and structure of the solid ablated, but are characteristic of the dynamics of the plasma in which the cluster ions are formed. Our detection of sulfur from pink MnS even without ablation, and the lower thermal stabilities of manganese sulfides relative to those of the later transition metals, are consistent with our postulate that the different surface chemistries of the two forms of MnS have different effects in the plasma where the clusters are assembled. The more stable green MnS gives a richer collection of cluster anions, and is more comparable with the $[M_xS_y]^-$ ions of the later transition metals. But even green MnS is subject to decomposition, and aged samples give decreased yields of the high mass $[Mn_xS_y]^-$ ions.

In this context we note similarities between the laser ablation of iron and manganese sulfides. The negative ions $[Fe_xS_y]^-$ formed on laser ablation of $KFeS_2$ showed a separate sulfur-rich distribution,[4] and it is known that iron sulfides generate surface sulfur.

Cluster compositions

The three series of cluster ions, $[Mn_xS_x]^-$, $[Mn_xS_{x+1}]^-$ and $[Mn_xS_xO]^-$, up to $x = 22$ with few absences, reveal a clear and definite pattern of stability for these compositions. This pattern raises various questions about the nature and basis of the stability demonstrated; for example, one question is why other compositions in the ion map of Fig. 2 are not observed. Before approaching these questions we compare our distribution of manganese sulfide clusters with the collections of gaseous manganese oxide and manganese sulfide clusters reported by others from related experiments.

Recently, Zhang *et al.*[23] generated negative ions $[Mn_xS_y]^-$ by laser ablation of a mixture of Mn (s) and S (s) (3:1 molar ratio), followed by expansion cooling in pulsed helium. The ions were monitored by time-of-flight mass spectrometry, and, after mass selection, their photoelectron (PE) spectra were measured. The distribution of $[Mn_xS_y]^-$ generated this way was similar to ours, with $y = x$ and $y = x \pm 1$, but $[Mn_{10}S_{10}]^-$ was the largest cluster detectable. The PE spectra could be measured for ions up to and including $[Mn_6S_6]^-$.

Remarkably similar distributions of $[Mn_xO_y]^+$ and $[Mn_xO_y]^-$ clusters have been observed in different experiments. When Mn was evaporated and reacted with adventitious sources of oxygen, followed by photoionisation and time-of-flight mass spectrometry,[24] the primary ions observed were $[Mn_xO_x]^+$, $x = 1$–13, and $[Mn_xO_{x+1}]^+$, $x = 4$–22. Laser ablation of $MnCO_3$ yielded sequences of anions $[Mn_xO_{x+1}]^-$ and $[Mn_xO_{x+2}]^-$.[25] These observations provide further support for the inherent stability of neutral species $[Mn_xE_x]^0$ and $[Mn_xE_{x+1}]^0$ E = O or S, which appear as negative ions after electron attachment in our experiments, and as positive ions after photoionisation.

Since the compositions of the oxide and sulfide clusters of manganese are the same, it is curious that in our experiments only one O atom substitutes for S (see Fig. 2). This is probably a consequence of the restricted availability of oxygen (as adventitious oxygen, from water) in our experiments, and we would expect that under different conditions clusters of the type $[Mn_xS_yO_z]^{\pm}$ could be formed, with $y + z = x$, $x \pm 1$.

The consistency between the different experimental methods for preparation shows that our distribution of compositions, $[Mn_xS_x]^-$ and $[Mn_xS_{x+1}]^-$, reflects fundamental stability, with the implication of a geometrical principle which favours these compositions. However, it is possible that the formation conditions are also influential. It is generally believed that negative ions are formed by attachment of low energy electrons to neutral species in the cooling plasma. Thus the well defined pattern of anions in Fig. 2 could also reflect the compositions of the neutral clusters which are best able to compete for electrons in the plasma, that is the clusters with the largest electron affinities. Zhang *et al.*[23] have estimated the electron affinities (EA) of clusters up to $[Mn_6S_6]$ from the PES data, but there is no evident correlation between the larger EA values and abundances of $[Mn_xS_y]^-$ ions in their spectra or in ours.

Density functional (DF) theory provides a powerful computational method for determination of the electronic structures of metal chalcogenide clusters, and in the following paper[26] we describe extensive calculations applied to the unresolved questions of electronic structure, geometrical structure and stability, for the $[Mn_xS_y]$ clusters.

Finally we note that the distribution of Fig. 2 complies with (and strongly supports) the electron population pattern noted for $[M_xS_y]^-$ clusters for metals ranging from V to Cu.[4,6,11] The normalised valence electron population (N_e) for $[M_xS_y]$ is defined as the total number of valence electrons for M and S (each S contributing 6e), per metal atom: that is, $N_e = [x$ (number of M valence electrons) + $6y]/x$. The pattern for all observed $[M_xS_y]^-$ clusters is that N_e is largely independent of the identity of M and of x.

Conclusion

Green MnS is the preferred solid for the generation of gaseous $[Mn_xS_y]^-$ clusters by laser ablation. Artefacts at the surface of the solid, especially excess sulfur which is more prevalent at the surface of pink MnS, influence the distributions of ions formed on laser ablation of the solid. The $[Mn_xS_y]^-$ clusters may incorporate adventitious oxygen. The relationship between cluster stability and composition occurs as well defined continuous series of ions with the compositions $[Mn_xS_x]$, $[Mn_xS_{x+1}]$ and $[Mn_xS_xO]$, without strong evidence that any particular compositions are substantially more stable than the others. It is argued that these stability series are fundamental to MnS cluster chemistry because they are largely independent of the charge of the observed ions and of the formation processes.

Like other anions, the $[Mn_xS_y]^-$ clusters are not very reactive, and are not oxidised by N_2O. However they do react with H_2S, adding one or two S atoms and forming some ions in the new series $[Mn_xS_{x+2}]^-$ ($x = 4$–8), and also protonating the anions.

The degree to which this gas phase chemistry can be applied to synthesis in condensed phases is yet to be determined. We

note that there are relatively few reports of Mn chalcogenide and polychalcogenide compounds,[27–31] and a small number of reports of Mn thiolates.[32–36] In a reaction which has some similarity with the gaseous reactions reported here, Rauchfuss and co-workers[37] have reacted Mn metal with S_8 in *N*-methylimidazole.

Acknowledgements

This research is supported by the Australian Research Council. K. J. F. acknowledges the award of a National Research Fellowship.

References

1 J. H. El Nakat, I. G. Dance, K. J. Fisher, D. Rice and G. D. Willett, *J. Am. Chem. Soc.*, 1991, **113**, 5141.
2 J. H. El Nakat, I. G. Dance, K. J. Fisher and G. D. Willett, *Inorg. Chem.*, 1991, **30**, 2957.
3 H. J. El-Nakat, I. G. Dance, K. J. Fisher and G. D. Willett, *J. Chem. Soc., Chem. Commun.*, 1991, 746.
4 J. H. El Nakat, K. J. Fisher, I. G. Dance and G. D. Willett, *Inorg. Chem.*, 1993, **32**, 1931.
5 I. G. Dance and K. J. Fisher, *Prog. Inorg. Chem.*, 1994, **41**, 637.
6 I. G. Dance and K. J. Fisher, *Mater. Sci. Forum*, 1994, **152**, 137.
7 I. G. Dance, K. J. Fisher and G. D. Willett, *Angew. Chem., Int. Ed. Engl.*, 1995, **34**, 201.
8 I. G. Dance, K. J. Fisher and G. D. Willett, *J. Chem. Soc., Chem. Commun.*, 1995, 975.
9 I. G. Dance, K. J. Fisher and G. D. Willett, *Inorg. Chem.*, 1996, **35**, 4177.
10 K. J. Fisher, I. G. Dance and G. D. Willett, *Rapid Commun. Mass Spectrom.*, 1996, **10**, 106.
11 K. J. Fisher, I. G. Dance, G. D. Willett and M. Yi, *J. Chem. Soc., Dalton Trans.*, 1996, 709.
12 K. J. Fisher and I. G. Dance, *Polyhedron*, 1997, in the press.
13 H. Wiedemeier and P. W. Gilles, *J. Chem. Phys.*, 1965, **42**, 2765.
14 G. Brauer, *Handbook of Preparative Inorganic Chemistry*, Academic Press, New York, London, 1963.
15 F. Jellinek, *Inorganic Sulfur Chemistry*, ed. G. Nickless, Elsevier, Amsterdam, 1968, pp. 669–747
16 F. Hulliger, *Struct. Bonding* (*Berlin*), 1968, **4**, 83.
17 R. D. W. Kemmitt, *Comprehensive Inorganic Chemistry*, Pergamon, Oxford, 1968, p. 813.
18 L. Corliss, N. Elliott and J. Hastings, *Phys. Rev.*, 1956, **104**, 924.
19 D. R. Huffman and R. L. Wild, *Phys. Rev.*, 1966, **148**, 526.
20 D. C. Parent, *Chem. Phys. Lett.*, 1991, **183**, 45.
21 D. Feldmann, R. Rackwitz, H. J. Kaiser and E. Heinecke, *Z. Naturforsch., Teil A*, 1977, **32**, 600.
22 M. R. Nimlos and G. B. Ellison, *J. Phys. Chem.*, 1986, **90**, 2574.
23 N. Zhang, H. Kawamata, A. Nakajima and K. Kaya, *J. Chem. Phys.*, 1996, **104**, 36.
24 P. J. Ziemann and A. W. Castleman, *Phys. Rev. B*, 1992, **46**, 13 480.
25 X. G. Zhang, personal communication, 1995.
26 I. G. Dance and K. J. Fisher, following paper.
27 D. Coucouvanis, P. Patil, M. G. Kanatzidis, B. A. Detering and N. C. Baenziger, *Inorg. Chem.*, 1985, **24**, 24.
28 R. L. Bedard, S. T. Wilson, L. D. Vail, J. M. Bennett and E. M. Flanigen, *Zeolites: Facts, Figures, Future*, eds. P. A. Jacobs and R. A. van Santen, Elsevier, Amsterdam, 1989, pp. 375–387.
29 H. O. Stephan, C. Chen, G. Henkel, K. Griesar and W. Haase, *J. Chem. Soc., Chem. Commun.*, 1993, 886.
30 H. O. Stephan and G. Henkel, *Angew. Chem., Int. Ed. Engl.*, 1994, **33**, 2322.
31 H. O. Stephan, M. G. Kanatzidis and G. Henkel, *Angew. Chem., Int. Ed. Engl.*, 1996, **35**, 2135.
32 J. L. Seela, K. Folting, R. J. Wang, J. C. Huffman, G. Christou, H. R. Chang and D. N. Hendrickson, *Inorg. Chem.*, 1985, **24**, 4454.
33 J. L. Seela, J. C. Huffman and G. Christou, *J. Chem. Soc., Chem. Commun.*, 1985, 58.
34 A. D. Watson, C. P. Rao, J. R. Dorfman and R. H. Holm, *Inorg. Chem.*, 1985, **24**, 2820.
35 C. P. Rao, J. R. Dorfman and R. H. Holm, *Inorg. Chem.*, 1986, **25**, 428.
36 P. P. Power and S. C. Shoner, *Angew. Chem., Int. Ed. Engl.*, 1991, **30**, 330.
37 S. Dev, E. Ramli, T. B. Rauchfuss and S. R. Wilson, *Inorg. Chem.*, 1991, **30**, 2514.

Received 4*th February* 1997; *Paper* 7/00820A